Neurobiology of Disease 103 (2017) 11–23

Contents lists available at ScienceDirect

Neurobiology of Disease

journal homepage: www.elsevier.com/locate/ynbdi

Long-term effect of neonatal inhibition of APP gamma-secretase on hippocampal development in the Ts65Dn mouse model of Down syndrome

Fiorenza Stagni [a,1], Alessandra Raspanti [b,1], Andrea Giacomini [a,1], Sandra Guidi [a], Marco Emili [a], Elisabetta Ciani [a], Alessandro Giuliani [c], Andrea Bighinati [d], Laura Calzà [d], Jacopo Magistretti [b], Renata Bartesaghi [a,*]

[a] Department of Biomedical and Neuromotor Sciences, University of Bologna, Bologna, Italy
[b] Department of Biology and Biotechnology "L. Spallanzani", University of Pavia, Pavia, Italy
[c] Department of Veterinary Medical Sciences,University of Bologna, Bologna, Italy
[d] Health Sciences and Technologies - Interdepartmental Center for Industrial Research (HST-ICIR), University of Bologna, Bologna, Italy

ARTICLE INFO

Article history:
Received 5 September 2016
Revised 9 March 2017
Accepted 26 March 2017
Available online 28 March 2017

Keywords:
Down syndrome
Neonatal pharmacotherapy
APP
Gamma-secretase
Hippocampal development

ABSTRACT

Neurogenesis impairment is considered a major determinant of the intellectual disability that characterizes Down syndrome (DS), a genetic condition caused by triplication of chromosome 21. Previous evidence obtained in the Ts65Dn mouse model of DS showed that the triplicated gene APP (amyloid precursor protein) is critically involved in neurogenesis alterations. In particular, excessive levels of AICD (amyloid precursor protein intracellular domain) resulting from APP cleavage by gamma-secretase increase the transcription of Ptch1, a Sonic Hedgehog (Shh) receptor that keeps the mitogenic Shh pathway repressed. Previous evidence showed that neonatal treatment with ELND006, an inhibitor of gamma-secretase, reinstates the Shh pathway and fully restores neurogenesis in Ts65Dn pups. In the framework of potential therapies for DS, it is extremely important to establish whether the positive effects of early intervention are retained after treatment cessation. Therefore, the goal of the current study was to establish whether early treatment with ELND006 leaves an enduring trace in the brain of Ts65Dn mice. Ts65Dn and euploid pups were treated with ELND006 in the postnatal period P3-P15 and the outcome of treatment was examined at ~one month after treatment cessation. We found that in treated Ts65Dn mice the pool of proliferating cells in the hippocampal dentate gyrus (DG) and total number of granule neurons were still restored as was the number of pre- and postsynaptic terminals in the stratum lucidum of CA3, the site of termination of the mossy fibers from the DG. Accordingly, patch-clamp recording from field CA3 showed functional normalization of the input to CA3. Unlike in field CA3, the number of pre- and postsynaptic terminals in the DG of treated Ts65Dn mice was no longer fully restored. The finding that many of the positive effects of neonatal treatment were retained after treatment cessation provides proof of principle demonstration of the efficacy of early inhibition of gamma-secretase for the improvement of brain development in DS.

1. Introduction

During the last few years, there has been a growing interest in the field of pharmacotherapies for intellectual disability in Down syndrome (DS) (see (Costa and Scott-McKean, 2013, Gardiner, 2015)), a genetic condition due to triplication of chromosome 21. To this purpose, mouse models have been exploited among which the Ts65Dn mouse, a model that recapitulates numerous features of trisomy 21 (Reeves, 2006), is the most widely used. The developmental alterations in the brain of Ts65Dn mice are due to perturbation of numerous pathways. Accordingly, studies that have used quite different pharmacological approaches in the Ts65Dn mouse model show that it is possible to ameliorate or even rescue the structural and behavioral deficits that characterize the Ts65Dn model of DS (see(Costa and Scott-McKean, 2013, Gardiner, 2015)). Most of these studies have been carried out in adulthood, a time at which neurogenesis and neuron maturation are well off. Neurogenesis and connectivity alterations are the major structural defects of the DS brain (see (Bartesaghi et al., 2011, Dierssen, 2012). Since these processes take place prenatally and in the early postnatal period, these periods represent critical windows of opportunity for the rescue of brain development. Indeed, studies in the Ts65Dn model show that pre- and early postnatal pharmacotherapies may have a

* Corresponding author at: Department of Biomedical and Neuromotor Sciences, Physiology Building, Piazza di Porta San Donato 2, I-40126 Bologna, BO, Italy.
E-mail address: renata.bartesaghi@unibo.it (R. Bartesaghi).
[1] Contributed equally to the work.
Available online on ScienceDirect (www.sciencedirect.com).

http://dx.doi.org/10.1016/j.nbd.2017.03.012

very large effect on neurogenesis, connectivity and behavior, being able, in some instances, to fully restore brain development (see (Stagni et al., 2015)). The advantage of preclinical studies is that mouse models provide the unique possibility to test a variety of different compounds. Identification of a panel of effective compounds in mouse models will increase the spectrum of possibilities to discover a therapy that is effective in individuals with DS.

Various studies have clearly shown that the Sonic Hedgehog pathway, a crucial pathway for brain morphogenesis and neural precursor proliferation, is altered in DS (Roper et al., 2006; Trazzi et al., 2011; Trazzi et al., 2013). This alteration can be ascribed to a cascade of events stemming from amyloid precursor protein (APP) triplication and culminating into overexpression of Patched 1 (Ptch1), the repressor of this pathway (Trazzi et al., 2011; Trazzi et al., 2013). In particular, cleavage of the APP-derived carboxy-terminal fragments (CTFs) by the enzyme gamma-secretase gives origin to the amyloid precursor protein intracellular domain (AICD) and either p3 or beta-amyloid (Abeta). In the trisomic brain, due to excessive APP expression there are excessive AICD levels that, in turn, increase the transcription of Ptch1 (Trazzi et al., 2011; Trazzi et al., 2013). It is important to observe that Ptch1 over-expression is present in the DS brain starting from fetal life stages (Trazzi et al., 2011), which prospects the possibility that derangement of the Shh pathway may be an important determinant of neurogenesis reduction and brain hypocellularity. During the last few years, various selective APP gamma-secretase inhibitors have been developed by ELAN Inc. (Basi et al., 2010), as strategic tools to reduce Abeta levels in Alzheimer's disease. Among these, ELND006 (ELN) is a gamma-secretase inhibitor which retains selectivity and incorporates improved drug-like properties (Basi et al., 2010; Probst et al., 2013). In a previous study we obtained evidence that neonatal treatment with this inhibitor of gamma-secretase was able to reinstate the functionality of the Shh pathway in the Ts65Dn mouse model of DS and that this effect led to restoration of neurogenesis and cellularity in the hippocampal dentate gyrus (Giacomini et al., 2015). These animals were treated from postnatal day 3 (P3) to postnatal day 15 (P15), *i.e.* the period of maximum neurogenesis in the hippocampal dentate gyrus, and were examined at the end of treatment. Since treatment was administered during the most critical time window for hippocampal development, it is possible that the dentate gyrus would remain in its restored state after treatment cessation. Yet, granule neurons are continuously added to the dentate gyrus and maturation of granule neurons requires 2–3 months. Unless treatment has effects that span beyond its cessation, its beneficial effects may tend to extinguish with time. The half-life of the effects of ELN has been shown to be in the range of 12–24 h (Brigham et al., 2010). Therefore, its direct effect on APP processing and, thus, Ptch1 levels, are expected to extinguish in a relatively short time. However, a treatment schedule of 13 days may induce secondary effects on signaling pathways that, if retained with time, may cause long-term effects even after treatment cessation.

In the framework of studies aimed at identifying therapies for intellectual disability in DS it is of paramount importance to establish not only the efficacy of the tested therapies but also the duration of their effects. This knowledge may help to choose the compound/s most suitable to be tested in clinical trials. Therefore, the goal of the current study was to establish whether neonatal treatment with ELN leads to enduring restoration of hippocampal development.

2. Methods

2.1. Colony

Female Ts65Dn mice carrying a partial trisomy of chromosome 16 (Reeves et al., 1995) were obtained from Jackson Laboratories (Bar Harbour, ME, USA) and the original genetic background was maintained by mating them with C57BL/6JEi x C3SnHeSnJ (B6EiC3) F1 males. Animals were genotyped as previously described (Reinholdt et al., 2011). The day of birth was designated postnatal day zero (P0). The animals' health and comfort were controlled by the veterinary service. The animals had access to water and food *ad libitum* and lived in a room with a 12:12 h dark/light cycle. Experiments were performed in accordance with the Italian and European Community law for the use of experimental animals and were approved by Bologna University Bioethical Committee. In this study all efforts were made to minimize animal suffering and to keep the number of animals used to a minimum.

2.2. Experimental protocol

We previously found that a dose of 30 mg/kg of ELND006 (ELN; gift by ELAN Inc., USA) from postnatal day 3 (P3) to postnatal day 15 (P15) had no acute effect on mice viability (Giacomini et al., 2015). However, we found here that euploid and Ts65Dn mice treated with this dose exhibited a higher mortality rate (death rate = 30–40%) after weaning. For this reason, we decided to reduce the dose of ELN. In a pilot experiment we found that a 20 mg/kg dose did not increase the mortality rate and was able to reinstate cell proliferation in the dentate gyrus of Ts65Dn mice ($n = 4$–5 mice for each experimental group; data not shown), similarly to the dose of 30 mg/kg. Therefore, in the current study we treated mice with a dose of 20 mg/kg. Euploid ($n = 20$) and Ts65Dn ($n = 11$) mice received a daily subcutaneous injection of ELN (dose 20 mg/kg) dissolved in the vehicle (25% PEG300, 25% ethylen glycol, 25% cremophor, 15% ethanol, 10% propanol) from P3 to P15. Age-matched euploid ($n = 19$) and Ts65Dn ($n = 10$) mice were injected with the vehicle. These mice will be called here untreated mice. Each treatment group had approximately the same composition of males and females. On P45-P50 mice were weighed, sacrificed, the brain was quickly removed and weighed. These mice will be called here P45 mice (Fig. 1A). The left hemisphere was fixed by immersion in PFA 4%, frozen and used for immunohistochemistry. The right hemisphere was kept at −80 °C and used for western blotting. The number of animals used for each of the experimental procedures described below is specified in the figure legends. Other groups of mice were treated from P3 to P15 with either ELN (20 mg/kg) (euploid: $n = 8$; Ts65Dn: $n = 4$) or vehicle (euploid: $n = 9$; Ts65Dn: $n = 7$) and at 30–45 days of age were used for electrophysiological recordings from field CA3 (Fig. 1A).

2.3. Histological procedures

The left hemisphere was cut with a freezing microtome in 30-μm-thick coronal sections that were serially collected in anti-freezing solution (30% glycerol; 30% ethylen-glycol; 10% PBS10X; 0.02% sodium azide; MilliQ to volume) and used for immunohistochemistry for Ki-67, synaptophysin (SYN) and postsynaptic density protein-95 (PSD-95).

2.3.1. Ki-67 immunohistochemistry

One out of 6 sections were taken starting from the beginning to the end of the hippocampal formation ($n = 16$–20 sections). Sections were incubated overnight at 4 °C with rabbit monoclonal anti-Ki-67 antibody (1:100; Thermo Scientific). Section were then incubated for 2 h with a Cy3 conjugated anti-rabbit IgG (1:200; Jackson Immunoresearch). Sections were counterstained with Hoechst 33342 in order to label cell nuclei.

2.3.2. SYN and PSD-95 immunohistochemistry

Free-floating sections ($n = 4$–6 per animal) from the hippocampal formation were submitted to fluorescence immunohistochemistry for SYN and PSD-95. Sections were incubated for 24 h at 4 °C with mouse monoclonal anti-SYN (SY38) antibody (Millipore-Biomanufacturing and Life Science Research, Billerica, MA, USA) or rabbit polyclonal anti-PSD-95 antibody (Abcam) both diluted 1:1000. Sections were then incubated for 2 h with a FITC-conjugated anti-mouse antibody or with a CY3-conjugated anti-rabbit (Jackson Laboratory) antibody both diluted 1: 200.

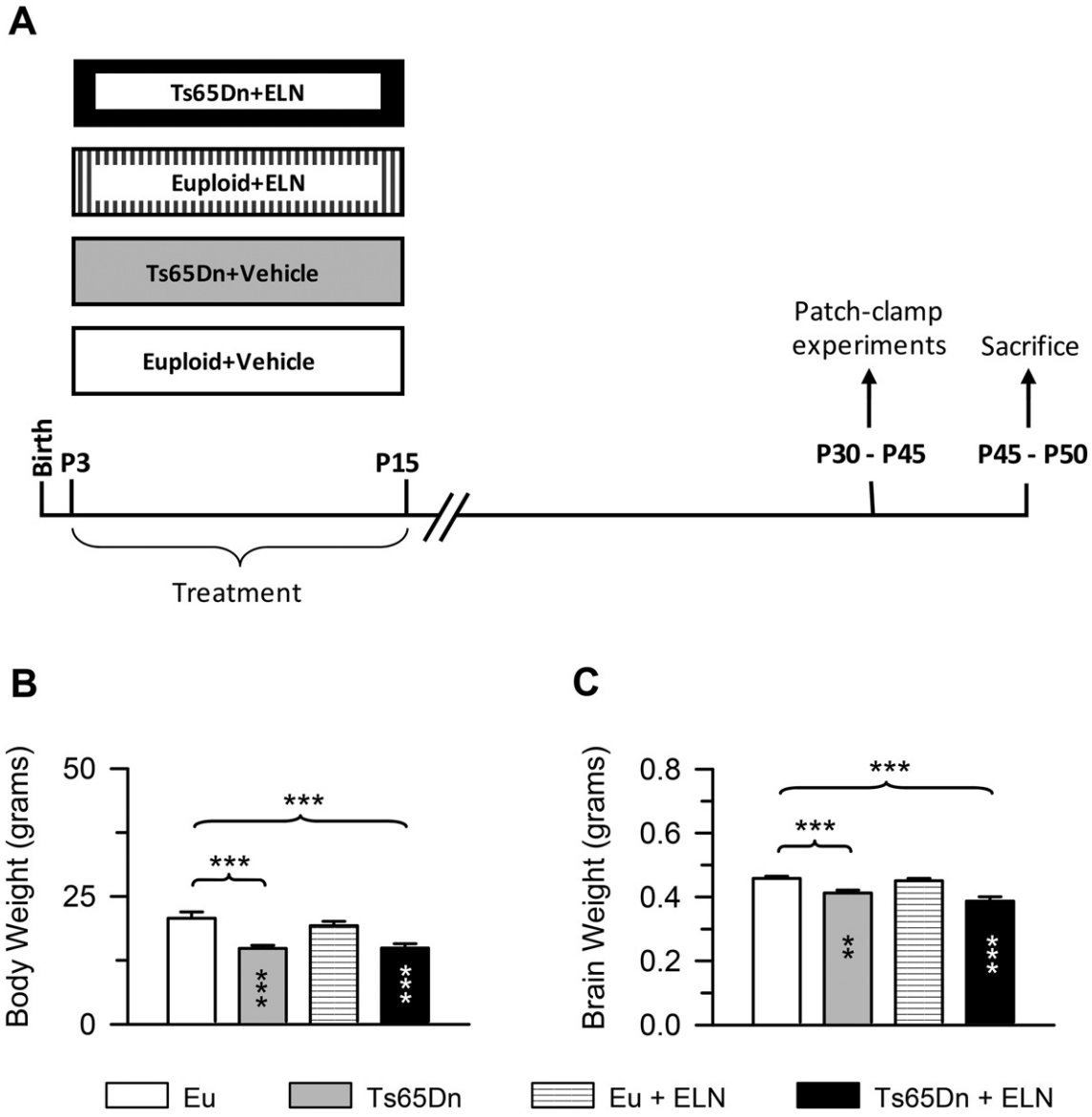

Fig. 1. Effect of treatment with ELN on the body and brain weight. A: Experimental protocol. Euploid and Ts65Dn mice received a daily injection of either vehicle (Eu + Vehicle; Ts65Dn + Vehicle) or ELND006 (Eu + ELN; Ts65Dn + ELN) from postnatal (P) day 3 to P15. Some mice were killed on P30-P45 and used for electrophysiological recordings from CA3. Other mice were killed on P45-P50. The brains of these mice were used for immunohistochemistry and western blotting. B, C: Body (B) and brain (C) weight (mean ± SE) in grams of euploid and Ts65Dn mice that received ELN or vehicle in the period P3-P15, measured on postnatal days P45-P50. Untreated euploid mice: $n = 19$; untreated Ts65Dn mice: $n = 10$; treated euploid mice: $n = 20$; treated Ts65Dn mice: $n = 11$. $^{***}p < 0.001$ (Fisher LSD test). Black asterisks in the gray bar indicate a difference between untreated Ts65Dn mice and treated euploid mice; white asterisks in the black bar indicate a difference between treated Ts65Dn mice and treated euploid mice. Abbreviations: ELN, ELND006; Eu, Euploid.

2.4. Measurements

2.4.1. Image acquisition

Immunofluorescence images of sections processed for Ki-67 were taken with a Nikon Eclipse TE 2000-S inverted microscope (Nikon Corp., Kawasaki, Japan), equipped with a Nikon digital camera DS 2MBWc. Immunofluorescence images of sections processed for SYN and PSD-95 immunohistochemistry were taken with a LEICA TCS SL confocal microscope. Measurements were carried out using Image Pro Plus software (Media Cybernetics, Silver Spring, MD 20910, USA).

2.4.2. Number of Ki-67-positive cells

Quantification of Ki-67-labeled nuclei in the dentate gyrus (DG) was conducted in every 6th section throughout the whole extent of the DG using a Nikon Eclipse TE 2000-S microscope (objective ×40, NA 0.75; final magnification ×400). A modified unbiased stereology protocol for quantification of proliferating cells (Malberg et al., 2000; Kempermann and Gage, 2002; Tozuka et al., 2005) was used. All Ki-67-labeled cells located in the granule cell and subgranular layers were counted along the entire z axis (1 μm steps) of each section. To avoid oversampling errors, the nuclei intersecting the uppermost focal plane were excluded. The total number of Ki-67-labeled cells per animal was determined and multiplied by six to obtain the total estimated number of cells per DG. We additionally evaluated the mean number of Ki-67-positive cells per section by dividing the number of counted cells by the number of sampled sections.

2.4.3. Synaptic terminals

Images of sections immunoprocessed for SYN or PSD-95 were acquired with a confocal microscope (Nikon Ti-E fluorescence microscope coupled with an A1R confocal system, Nikon). In each section three images from the molecular layer of the DG and the stratum lucidum of field CA3 were captured and the density of individual puncta exhibiting SYN

or PSD-95 immunoreactivity was evaluated as previously described (Guidi et al., 2013; Stagni et al., 2013).

2.4.4. Stereology of the DG

Unbiased stereology was performed on Hoechst-stained sections. The optical disector method was used to obtain cell density, and the Cavalieri principle was used to estimate volume of the granule cell layer of the DG (West and Gundersen, 1990). In P45 mice, one DG is represented in 90–110 30-μm-thick sections. To include 16–18 sections, every 6th section was selected, beginning at a random position within the first 6 sections. For determination of the granule cell number, granule cell nuclei were counted with a ×63 oil objective (NA 1.32). In order to obtain granule cell numerical density, cells were counted in 30 × 30 counting frames spaced in a 100 μm square grid superimposed over each section. Cells that intersected the uppermost focal (exclusion) plane and those that intersected the exclusion boundaries of the unbiased sampling frame were excluded from counting. Cells that met the counting criteria through a 30 μm axial distance were counted according to the optical disector principle.

The neuron density (Nv) is given by

$$N_V = (\Sigma Q/\Sigma dis)/Vdis$$

where Q is the number of particles counted in the disectors, dis is the number of disectors and Vdis is the volume of the disector. For volume (Vref) estimation with the Cavalieri principle, in each sampled section, the area of the granule cell layer was measured by tracing its contours. The volume of the granule cell layer (Vref) was estimated (West and Gundersen, 1990) by multiplying the sum of the cross sectional areas by the spacing T between sampled sections (180 μm). The total number (N) of granule cells was estimated as the product of V_{ref} and the numerical density (Nv).

$$N = N_V \times V_{ref}$$

2.5. Western blotting

In homogenates of the hippocampal formation, total proteins were obtained as previously described (Trazzi et al., 2011). Proteins (50–80 μg) were subjected to electrophoresis on a 4–12% NuPAGE Bis-Tris Precast Gel (Novex, Life Technologies, Ltd., Paisley, UK) and transferred to a Hybond ECL nitrocellulose membrane (Amersham Life Science). The following primary antibodies were used: anti-Ptch1 (1:1000; Abcam), anti-p21 (1:500; Santa Cruz Biotechnology), anti-APP C-Terminal (1:2000; Sigma-Aldrich) and anti-GAPDH (1:5000; Sigma-Aldrich). Densitometric analysis of images digitized with ChemiDoc XRS + was performed with Image Lab software (Bio-Rad Laboratories, Hercules, CA, USA) and intensity for each band was normalized to the intensity of the corresponding GAPDH band.

2.6. Patch-clamp experiments

2.6.1. Preparation of slices

Mice (P30–P45) were anesthetised by inhalation of isoflurane (Merial Italia, Milan, Italy) and transcardially perfused with a cutting solution. The brain was quickly extracted under hypothermic conditions and submerged in ice-cold cutting solution. For the preparation of slices for the voltage-clamp recordings, the cutting solution was composed of (in mmol/l): 70 sucrose, 80 NaCl, 2.5 KCl, 26 $NaHCO_3$, 15 glucose, 7 $MgCl_2 \cdot 6\,H_2O$, 1 $CaCl_2 \cdot 2\,H_2O$, 1.25 $NaH_2PO_4 \cdot H_2O$. pH was 7.4 by saturation with 95% O_2, 5% CO_2. Two coronal cuts were made, in order to remove the anterior half and the occipital pole of the brain, and the piece thus obtained was laid on the posterior section plane. The tissue was blocked on the stage of a Microslicer DTK-1000 vibratome (Dosaka, Kyoto, Japan) using cyanoacrilate glue. Coronal slices of the hippocampus, 350-μm thick, were cut maintaining the tissue submerged in an ice-cold solution composed of (in mmol/l): 130 K gluconate, 15 KCl, 20 HEPES, 0.2 EGTA, 11 glucose. The use of this high-K + solution was found to improve neuron viability (Stephane Dieudonné, unpublished results). The slices were then transferred to a recovery chamber filled with a maintaining solution continuously bubbled with 95% O_2, 5% CO_2, at room temperature (21–22 °C) for at least 1 h before starting the recording. The maintaining solution for the voltage-clamp experiments was composed of (in mmol/l): 125 NaCl, 2.5 KCl, 26 $NaHCO_3$, 15 glucose, 1.3 $MgCl_2$, 2.3 $CaCl_2 \cdot 2\,H_2O$ e 1.25 $NaH_2PO_4 \cdot H_2O$.

2.6.2. Voltage-clamp recordings, drugs, and data analysis

Whole-cell, patch-clamp recordings from CA3 pyramidal neurons were carried out on acute slices of the dorsal hippocampus obtained as described above. The experimental set-up employed and the basic procedures followed were the same as described elsewhere (Castelli et al., 2007). Briefly, cells were visualized by means of an upright microscope (Axioskop 2 FS; Zeiss, Oberkochen, FRG) equipped with a ×60 water-immersion objective lens, differential-contrast optics, and a near-infrared charge-coupled device (CCD) camera. Slices were perfused with ACSF (continuously bubbled with 95% O_2, 5% CO_2) at a rate of about 1.5 ml/min. Patch pipettes were fabricated from thick-wall borosilicate glass capillaries (CEI GC 150-7.5; Harvard Apparatus, Edenbridge, UK) by means of a Sutter P-87 horizontal puller (Sutter Instruments, Novato, CA, USA). The pipette solution contained (in mmol/l): 150 CsF, 4 CsCl, 2 $MgCl_2$, 10 N-2-hydroxyethyl piperazine-N-2-ethanesulphonic acid (HEPES), 10 ethylene glycol-bis (β-aminoethyl ether) *N*,*N*,*N*′,*N*′-tetraacetic acid (EGTA), 2 adenosine 5′-triphosphate (ATP)-Na_2, 0.2 guanosine 5′-triphosphate (GTP)-Na, 2.5 lidocaine N-ethyl bromide (QX-314) (pH adjusted to 7.2 with CsOH). The patch pipettes had a resistance of 3–5 MΩ when filled with the above solution. Tight seals (>5 GΩ) and the whole-cell configuration were obtained by suction according to the standard technique (Hamill et al., 1981). Excitatory postsynaptic currents (EPSCs) were recorded at room temperature (21–22 °C) by means of an Axopatch 200B patch-clamp amplifier (Axon Instruments, Foster City, CA, USA). Series resistance (R_s) was evaluated on line by canceling the whole-cell capacitive transients evoked by −5-mV voltage square pulses with the amplifier built-in compensation section, and reading out the corresponding values. R_s was normally 5–12 MΩ and always <20 MΩ, and was compensated by ~90%. Current signals were acquired in gap-free modality with a personal computer interfaced to a Digidata 1322A interface (Axon Instr.) using the Clampex program of the pClamp 8.2 software package (Axon Instr.). Current signals were low-pass filtered at 5 kHz and digitized at 20 kHz. Miniature synaptic currents were recorded in the presence of tetrodotoxin (used to block voltage-gated Na + channels, and therefore the discharge of Na +-dependent action potentials) in the perfusing solution, so as to prevent spontaneous synaptic events due to presynaptic action potential firing. Tetrodotoxin (TTx) was purchased from Alomone Labs (Jerusalem, Israel). D-(−)-2-amino-5-phosphonopentanoic acid (APV; NMDA-receptor antagonist) and (2,3-dihydroxy-6-nitro-7-sulfamoyl-benzo[*f*]quinoxaline-2,3-dione) (NBQX; AMPA receptor antagonist) were purchased from Tocris (Bristol, UK). Drugs were preliminarily dissolved in H_2O and stored in concentrated aliquots at −20 °C. At the time of recording, the small aliquots were dissolved to the final concentrations (TTx: 1 μM; APV 50 μM; NBQX: 10 μM).

2.6.3. Data analysis

Results were off-line detected using an automated threshold routine in the LabView environment written and kindly provided by Dr. G. Biella (University of Pavia). All detected events were also visually inspected one-by-one for confirmation or rejection. To be considered a synaptic event the amplitude of the EPSC was required to be at least twice the noise amplitude: the events that showed a lower amplitude were ignored. Accepted events were then used to construct frequency

distribution diagrams of mEPSC amplitude. The EPSCs amplitude from whole-cell recordings were analyzed by means of the program Clampfit of pClamp 8.2 (Axon Instr.). Peak amplitude values of postsynaptic currents were analyzed with Origin 6.0 (MicroCal Software, Northampton, MA, USA) in order to build up frequency-distribution diagrams of the current recorded.

2.7. Statistical analysis

Data from single animals represented the unity of analysis. Results are presented as mean ± standard error of the mean (SE). Statistical analysis of all examined variables (with the exception of electrophysiological data) was carried out using a two-way ANOVA with genotype (euploid and Ts65Dn) and treatment (vehicle and ELN) as factors. *Post hoc* multiple comparisons were carried out using the Fisher least significant difference (LSD) test. Data were analyzed with IBM SPSS 22.0 software. For statistical analysis of the overall mEPSC frequency, a linear mixed model was used. The model has been fit using the Restricted or Residual Maximum Likelihood (REML). It calculated the average frequency keeping memory of the number of cells recorded in each animal of the same experimental group (95% confidence interval). Data were analyzed with the software R. version 3.2.3. For the analysis of the decay time constant (τdec) of mEPSC as a function of mEPSCs amplitude a linear regression analysis was used ($y = A + B * X$). The relative weight of each data point in the fitting procedure was made proportional to the number of events from which the corresponding average current had been obtained. Data were analyzed with the software Origin 6.0 using the Fit Linear function. For all analyses, a probability level of $p < 0.05$ was considered to be statistically significant.

3. Results

3.1. Long-term effect of treatment with ELN on body and brain weight

In order to obtain information on the general effect of neonatal treatment with ELN, we examined the effects of treatment on the body and brain weight of all mice used for immunohistochemistry and western blotting.

A two-way ANOVA on body weight showed no genotype x treatment interaction; an effect of genotype [$F(1,56) = 25.704$, $p \leq 0.000$] was shown, but no effect of treatment emerged. A *post hoc* LSD test showed that, consistently with previous evidence, untreated Ts65Dn mice had a reduced body weight in comparison with their euploid counterparts (Fig. 1B). Treatment with ELN did not affect the body weight of either Ts65Dn or euploid mice (Fig. 1B).

A two-way ANOVA on brain weight showed no genotype x treatment interaction; a significant effect of genotype [$F(1,56) = 33.463$, $p \leq 0.000$] but no effect of treatment. A *post hoc* LSD test showed that in untreated Ts65Dn mice the brain had a reduced weight in comparison with their euploid counterparts (Fig. 1C). Treatment had no effects on the brain weight on either Ts65Dn or euploid mice (Fig. 1C). This evidence suggests that neonatal treatment with ELN has no patent long-term adverse effects on animals' general conditions.

3.2. Long-term effect of treatment with ELN on cell proliferation and cellularity in the dentate gyrus

Since we had previously found that immediately after neonatal treatment with ELN there was restoration of the pool size of actively dividing granule cell precursors, we wondered whether this positive effect was retained after treatment cessation. To this purpose, we evaluated the number of cells that were immunopositive for Ki-67, an endogenous protein expressed by cycling cells over all phases of the cell cycle.

A two-way ANOVA on the number of Ki-67-positive cells per section in the DG showed a genotype × treatment interaction [$F(1,20) = 16.652$, $p = 0.001$], but no significant effect of genotype or treatment. A two-way ANOVA on total Ki-67-positive cells in the DG showed a genotype x treatment interaction [$F(1,20) = 23.164$, $p \leq 0.000$], but no effect of genotype or treatment emerged. A *post hoc* LSD test showed that untreated Ts65Dn mice had fewer Ki-67-positive cells per section (Fig. 2B) and a reduced total number of cells (Fig. 2C) than untreated euploid mice. In contrast, Ts65Dn mice that had been neonatally-treated with ELN had a similar number of Ki-67-positive cells per section (Fig. 2B) and a similar total cell number (Fig. 2C) as untreated euploid mice, indicating that the positive effect of treatment on precursor proliferation was retained with time. Unlike in Ts65Dn mice, in euploid mice treated with ELN there was a reduction in the number of Ki-67-positive cells per section (Fig. 2B) and total number of Ki-67-positive cells (Fig. 2C) in comparison with untreated euploid mice.

We stereologically examined the granule cell layer of the DG in order to establish whether the positive impact of treatment on the cellularity of the DG observed at P15 in Ts65Dn mice was retained after treatment cessation.

A two-way ANOVA on total number of granule cells showed a genotype × treatment interaction [$F(1,20) = 16{,}070$, $p \leq 0{,}000$] but not significant effect of genotype or treatment. A *post hoc* LSD test showed that untreated Ts65Dn mice had fewer granule cells than untreated euploid mice (Fig. 3B). In contrast, in Ts65Dn mice that had been neonatally-treated with ELN the number of granule cells underwent an increase and was similar to that of untreated euploid mice (Fig. 3B), indicating that the positive effect of treatment on total granule cell number was retained with time. Unlike in Ts65Dn mice, in euploid mice neonatally-treated with ELN there was a reduction in the total number of granule cells in comparison with untreated euploid mice (Fig. 3B).

3.3. Short- and long-term effects of neonatal treatment with ELN on CTFs levels

An important question regards the duration of the effects of ELN on the activity of gamma-secretase and hence, AICD levels after treatment cessation. Unfortunately, unlike in cultures of NPCs (Giacomini et al., 2015), in brain samples processed for western blotting, AICD levels resulted to be hardly detectable and we were able to detect an AICD band in 4% of all examined cases only. This small peptide (57 or 59 amino acids) has a very short half-life (about 5 min) (Cupers et al., 2001) and it is difficult to acquire pure AICD *in vitro* or detect its existence *in vivo* (Zheng et al., 2012). Thus, its degradation during brain removal may render it undetectable. Since AICD derives from the cleavage of the CTFs, inhibition of the activity of gamma-secretase reduces the levels of AICD but increase the levels of CTFs. Accordingly, in cultures of NPCs we found that following inhibition of gamma-secretase the reduction in AICD levels was accompanied by an increase in the levels of the CTFs (Giacomini et al., 2015). This suggests that an estimate of AICD levels can be obtained indirectly by quantifying the levels of the CTFs. Thus, in order to obtain information regarding the short- and long-term effect of treatment on AICD levels we evaluated the levels of the CTFs in mice aged 15 days used in our previous study (Giacomini et al., 2015) and in P45 mice of the current study.

A two-way ANOVA on CTFs levels in P15 mice showed no genotype x treatment interaction, but a main effect of both genotype [$F(1,20) = 15.071$, $p = 0.001$] and treatment [$F(1,20) = 30.874$, $p \leq 0.000$] was found. A *post hoc* LSD test showed that in the hippocampus of untreated Ts65Dn mice there were higher levels of CTFs in comparison to euploid mice (Fig. 4B). P15 Ts65Dn mice treated with ELN underwent an increase in the levels of CTFs in comparison with their untreated counterparts (Fig. 4B), which is consistent with the inhibitory action exerted by ELN on the activity of gamma-secretase.

A two-way ANOVA on CTFs levels in P45 mice showed no genotype x treatment interaction, a main effect of genotype [$F(1,28) = 30.081$, $p = 0.000$], but no significant effect of treatment. Similarly to P15, *post hoc* LSD test showed higher hippocampal levels of CTFs in P45 untreated

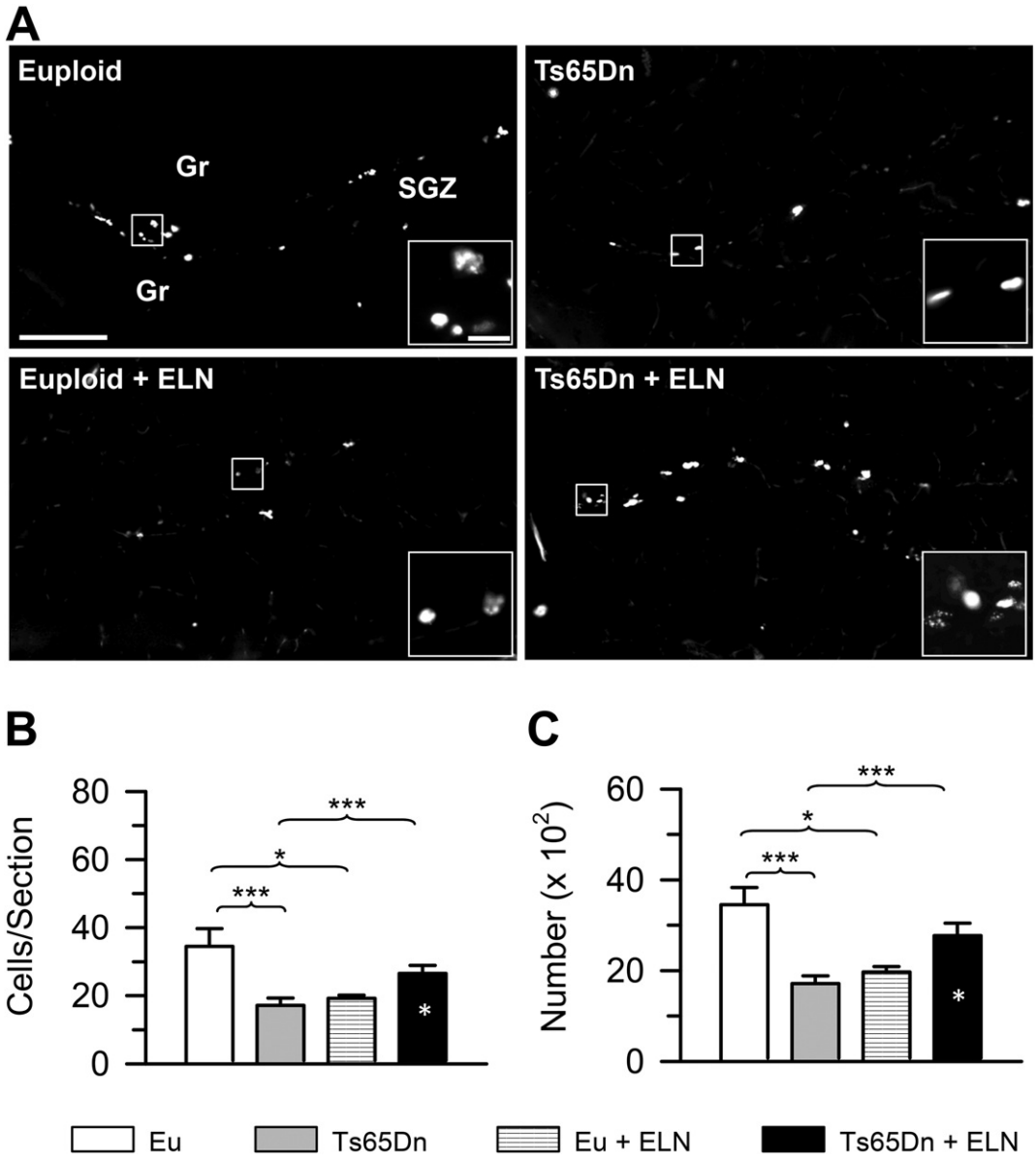

Fig. 2. Long-term effect of treatment with ELN on the size of the population of neural precursor cells in the dentate gyrus. A: Examples of sections processed for fluorescent immunostaining for Ki-67 from the dentate gyrus of untreated euploid and Ts65Dn mice and euploid and Ts65Dn mice treated with ELN. Examples of Ki-67-positive cells are indicated by the arrowheads. Calibrations = 200 μm (lower magnification) and 40 μm (higher magnification). B, C: Mean number of Ki-67-positive cells per section (B) and total number of Ki-67-positive cells (C) in the DG of treated and untreated Ts65Dn and euploid mice ($n = 6$ for each experimental group). Values represent mean ± SE. $^{*}p < 0.05$; $^{***}p < 0.001$ (Fisher LSD test). White asterisks in the black bar indicate a difference between treated Ts65Dn mice and treated euploid mice. Abbreviations: ELN, ELND006; Eu, Euploid; Gr, granule cell layer; SGZ, subgranular zone.

Ts65Dn mice in comparison with euploid mice (Fig. 4D). P45 Ts65Dn mice treated with ELN, however, had similar levels of CTFs as their untreated counterparts (Fig. 4D), indicating that the inhibition exerted by ELN on the activity of gamma-secretase does not outlast treatment cessation.

3.4. Long-term effects of neonatal treatment with ELN on Ptch1 levels

In order to establish whether neonatal treatment with ELN caused an enduring effect on Ptch1 levels in Ts65Dn mice, we evaluated the expression of Ptch1 in hippocampal homogenates of P45 mice that had been neonatally-treated with ELN or vehicle. Two-way ANOVA on hippocampal Ptch1 levels did not reveal a genotype x treatment interaction and no significant effects of both genotype and treatment emerged. *Post hoc* LSD test showed no statistical differences among the four experimental groups (Fig. 5A). This result indicate an age-related normalization of Ptch1 expression and suggest that the neurogenesis impairment still present in P45 Ts65Dn mice (Fig. 2) cannot be attributed to over-inhibition of the Shh pathway. Unlike in P15 mice (Giacomini et al., 2015), in both euploid and Ts65Dn P45 mice neonatally-treated with ELN, Ptch1 levels did not undergo a reduction (Fig. 5A).

Similarly to embryos and infants with Down syndrome, Ts65Dn mice exhibit higher brain levels of p21 (cip1/WAF1) (Engidawork et al., 2001; Park et al., 2010; Guidi et al., 2014), a cyclin-dependent kinase inhibitor that inhibits cell cycle progression. Since the results described above suggested that the reduced proliferation in untreated P45 Ts65Dn mice and its long-term normalization after treatment (Fig. 2) could not be ascribed to the Shh pathway, we wondered whether a change in p21 expression may contribute to modulate neurogenesis in treated Ts65Dn mice. Two way ANOVA on p21 hippocampal level showed a genotype x treatment interaction [$F(1,28) = 8.354$, $p = 0.007$], but no effects of genotype or treatment emerged. Confirming previous evidence (Guidi et al., 2014), a *post hoc* LSD showed that untreated Ts65Dn mice had higher hippocampal levels of p21 than euploid mice. Treatment caused

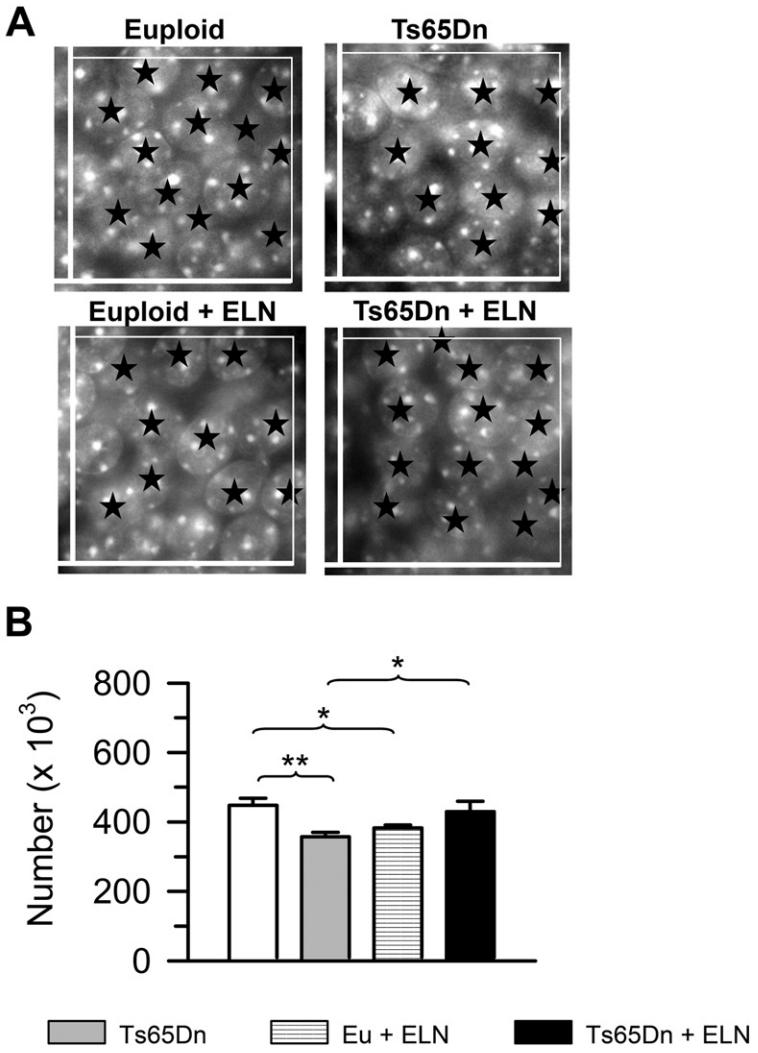

Fig. 3. Long-term effect of treatment with ELN on the number of granule neurons of the dentate gyrus. A: Representative images of Hoechst-stained sections of the granule cell layer of an animal from each experimental group. The sides of the superimposed optical disector are 30 μm in length. The stars indicate individual nuclei. Note that nuclei intersecting the exclusion sides (thick lines) were not counted. B: Total number of granule cells in untreated and treated euploid and Ts65Dn mice ($n = 6$ for each experimental group). Values (mean ± SE) refer to one hemisphere. $^{*}p < 0.05$; $^{**}p < 0.01$ (Fisher LSD test). Abbreviations: ELN, ELND006; Eu, Euploid.

a reduction in p21 levels in Ts65Dn mice although this effect was only marginally significant (Fig. 5C). In contrast, in treated euploid mice p21 levels underwent an increase in comparison with untreated euploid mice (Fig. 5C). This evidence provides a mechanistic link between the long-term restoration of precursor proliferation found in P45 treated Ts65Dn mice and the reduction in the number of neural precursors in treated euploid mice (Fig. 2).

3.5. Long-term effects of neonatal treatment with ELN on hippocampal synapses

Synaptophysin (SYN) is a synaptic vesicle glycoprotein that is a marker of presynaptic terminals and postsynaptic density protein-95 (PSD-95) is a postsynaptic scaffolding protein that is highly expressed in excitatory spines, and is a marker of postsynaptic regions. We counted the number of SYN and PSD-95 immunoreactive puncta in the middle molecular layer of the DG (the site of termination of the perforant path fibers from the entorhinal cortex) and the stratum lucidum of field CA3 (the site of termination of the granule cell axons, the mossy fibers), in order to establish whether neonatal treatment with ELN has a long-term effect on hippocampal synapses.

A two-way ANOVA on the number of SYN puncta in the molecular layer of the DG showed no genotype x treatment interaction; a main effect of genotype [$F(1,20) = 14.330$ $p \leq 0.001$] emerged, but there was no effect of treatment. A two-way ANOVA on the number of PSD-95 puncta in the molecular layer of the DG showed no genotype x treatment interaction; there was an effect of genotype [$F(1,20) = 46.893$, $p \leq 0.000$], but no effect of treatment. A *post hoc* LSD test showed that in the molecular layer of the DG, untreated Ts65Dn mice had fewer SYN (Fig. 6A) and PSD-95 (Fig. 6B) immunoreactive puncta in comparison with untreated euploid mice. In treated Ts65Dn mice the number of puncta was slightly larger in comparison with their untreated counterparts but this difference was not statistically significant. Consequently, treated Ts65Dn mice had fewer SYN (Fig. 6A) and PSD-95 (Fig. 6B) immunoreactive puncta in comparison with untreated euploid mice.

A two-way ANOVA on the number of SYN puncta in the stratum lucidum of field CA3 showed no genotype x treatment interaction but did show a significant effect of both genotype [$F(1,20) = 13.046$, $p \leq 0.002$] and treatment [$F(1,20) = 60.003$, $p \leq 0.000$]. A two-way ANOVA on the number of PSD-95 puncta in the field CA3 showed a genotype x treatment interaction [$F(1,20) = 8.181$, $p \leq 0.010$] and a main effect of both genotype [$F(1,20) = 22.792$, $p \leq 0.000$] and treatment [$F(1,20) = 9.432$, $p \leq 0.006$]. A *post hoc* LSD test showed that in the field CA3 untreated Ts65Dn mice had fewer SYN (Fig. 6C) and PSD-95 (Fig. 6D) immunoreactive puncta in comparison with untreated euploid mice. However, in treated Ts65Dn mice the number of SYN and PSD-95

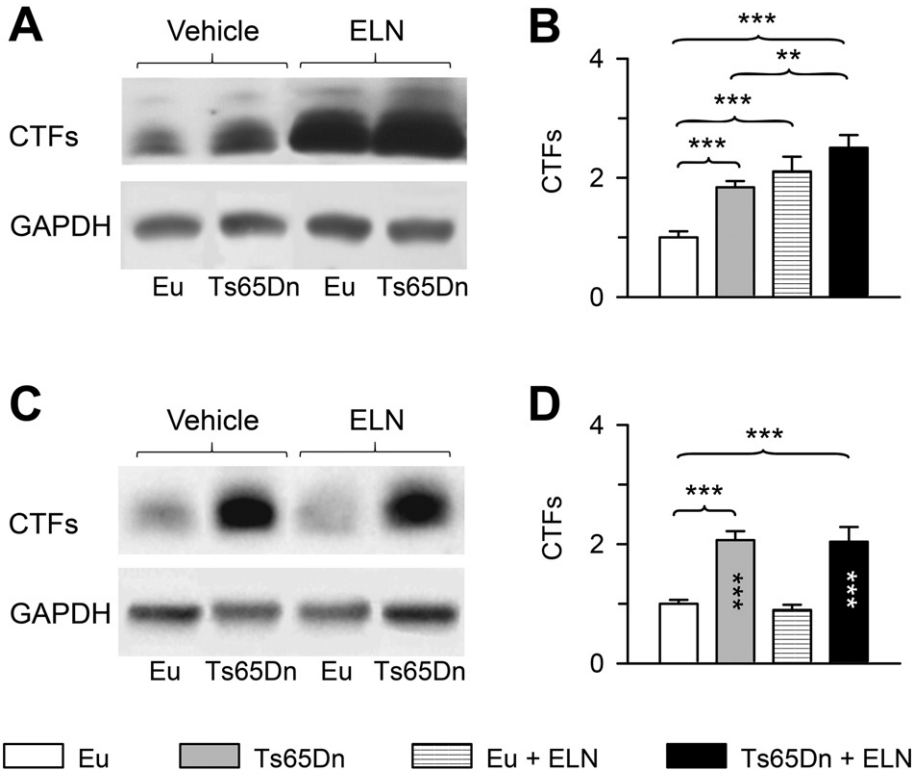

Fig. 4. Short- and long-term effect of treatment with ELN on CTFs levels. Western blot analysis of CTFs in the hippocampus of treated and untreated Ts65Dn and euploid mice ($n = 8$ for each experimental group). P15 and P45 mice were treated with ELN in the period P3-P15. A, C: Examples of western blot images of CTFs in P15 (A) and P45 (C) mice. B, D: Quantification of CTFs levels in P15 (B) and P45 (D) mice normalized to GAPDH. Values (mean ± SE) are expressed as fold difference in comparison with untreated euploid mice. $^{**}p < 0.01$; $^{***}p < 0.001$ (Fisher LSD test). Black asterisks in the gray bar indicate a difference between untreated Ts65Dn mice and treated euploid mice. White asterisks in the black bar indicate a difference between treated Ts65Dn mice and treated euploid mice. Abbreviations: ELN, ELND006; Eu, Euploid.

immunoreactive puncta was significantly larger in comparison with their untreated counterparts and was similar to or even larger than that of untreated euploid mice (Fig. 6C,D), indicating a long-term positive effect of neonatal treatment on DG-CA3 connections. An increase in the number of SYN immunoreactive puncta also took place in treated euploid mice in comparison with their untreated

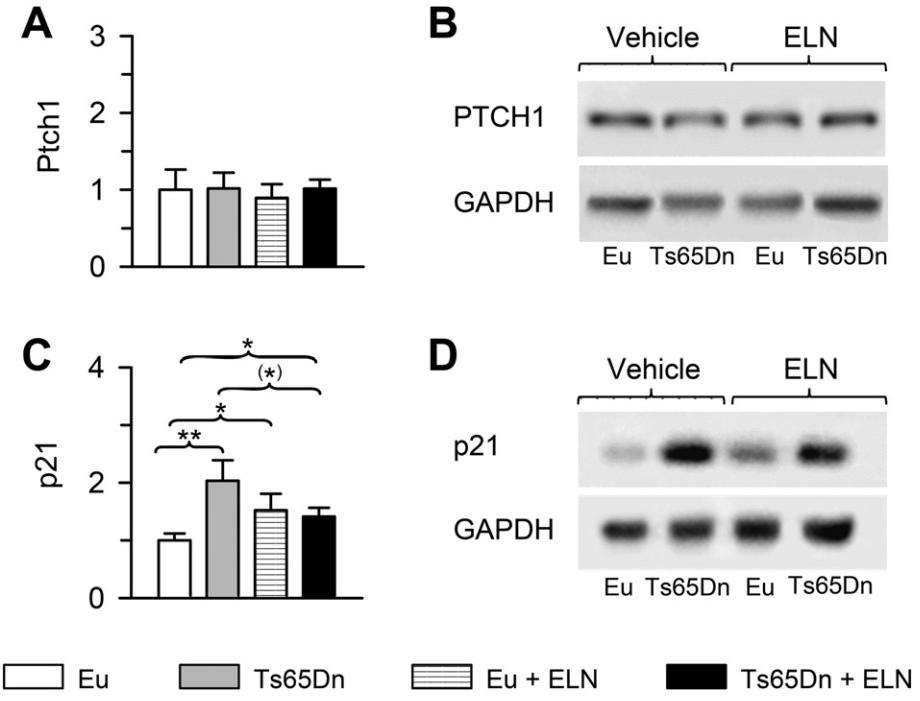

Fig. 5. Long-term effect of treatment with ELN on protein levels. Western blot analysis of Ptch1 and p21 in the hippocampus of treated and untreated Ts65Dn and euploid mice ($n = 8$ for each experimental group). A-D: Examples of western blot images of Ptch1 (B) and p21 (D) and quantification of Ptch1 (A) and p21 (C) levels normalized to GAPDH. Values (mean ± SE) are expressed as fold difference in comparison with untreated euploid mice. $(^{*})p < 0.06$; $^{*}p < 0.05$; $^{**}p < 0.01$ (Fisher LSD). Abbreviations: ELN, ELND006; Eu, Euploid.

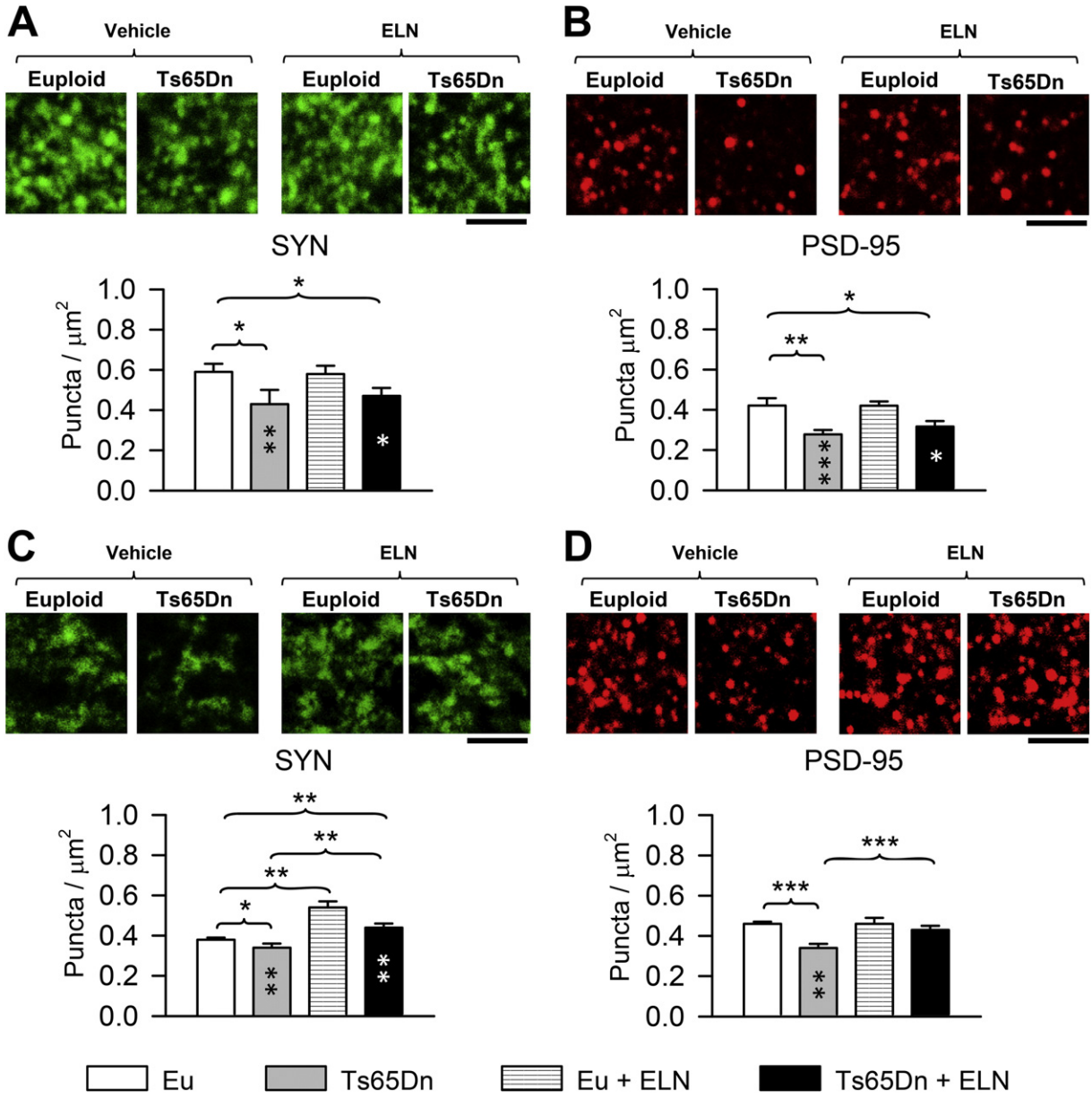

Fig. 6. Long-term effect of treatment with ELN on hippocampal synapses in Ts65Dn and euploid mice. A-D: Images in the panels at the top represent confocal microscope images of sections processed for SYN (A, C) and PSD-95 (B,D) immunofluorescence from the molecular layer of the DG (A, B) and the stratum lucidum of field CA3 (C, D) of an animal from each experimental group. Calibration = 5 µm. The histograms represent the number of puncta per µm^2 exhibiting SYN (A, C) and PSD-95 (B, D) immunoreactivity in the molecular layer of the DG (A, B) and the stratum lucidum of CA3 (C, D) of treated and untreated Ts65Dn and euploid mice ($n = 6$ for each experimental group). Values represent mean ± SE $^*p < 0.05$; $^{**}p < 0.01$; $^{***}p < 0.001$ (Fisher LSD test). Black asterisks in the gray bar indicate a difference between untreated Ts65Dn mice and treated euploid mice; white asterisks in the black bar indicate a difference between treated Ts65Dn mice and treated euploid mice. Abbreviations: ELN, ELND006; Eu, Euploid.

counterparts (Fig. 6C), with no change in the number of PSD-95 immunoreactive puncta (Fig. 6D).

3.6. Long-term effect of ELN on basal synaptic input to CA3 neurons

"Miniature" synaptic events reflect the spontaneous release of neurotransmitters from all presynaptic terminals converging on the recorded neuron. The frequency of these events is related to the total number of presynaptic terminals and the probability of release at each terminal. In order to functionally evaluate the basal excitatory synaptic input to CA3 pyramidal neurons, we recorded spontaneous miniature excitatory postsynaptic currents (mEPSCs) from individual CA3 pyramidal neurons by performing whole-cell, patch-clamp experiments in the voltage-clamp mode. Miniature events were recorded in the presence of tetrodotoxin (TTx, 1 µM) in the perfusing solution, in order to prevent spontaneous synaptic events due to presynaptic action-potential firing. In each cell, mEPSC activity was continuously recorded for a period of at least 5 min and up to 10 min. For mEPSC recording, the holding potential was set at −70 mV, a level that, under our experimental conditions, was close to the theoretical equilibrium potential of chloride ions (−71.5 mV), and therefore to the reversal potential of GABAergic currents: this allowed for mEPSC recording in virtual isolation from mIPSCs.

Fig. 7C shows examples of mEPSCs recorded, under the above conditions, in representative cells from untreated and ELN-treated euploid and Ts65Dn mice. No spontaneous synaptic events were observable any longer after application of the glutamatergic inhibitors NBQX (10 µM) + APV (50 µM) ($n = 4$ cells; not shown). Due to baseline noise levels normally observed at −70 mV, events of <10 pA in peak amplitude were ignored. Accepted events were then used to construct frequency-distribution diagrams of mEPSC amplitude. Data were

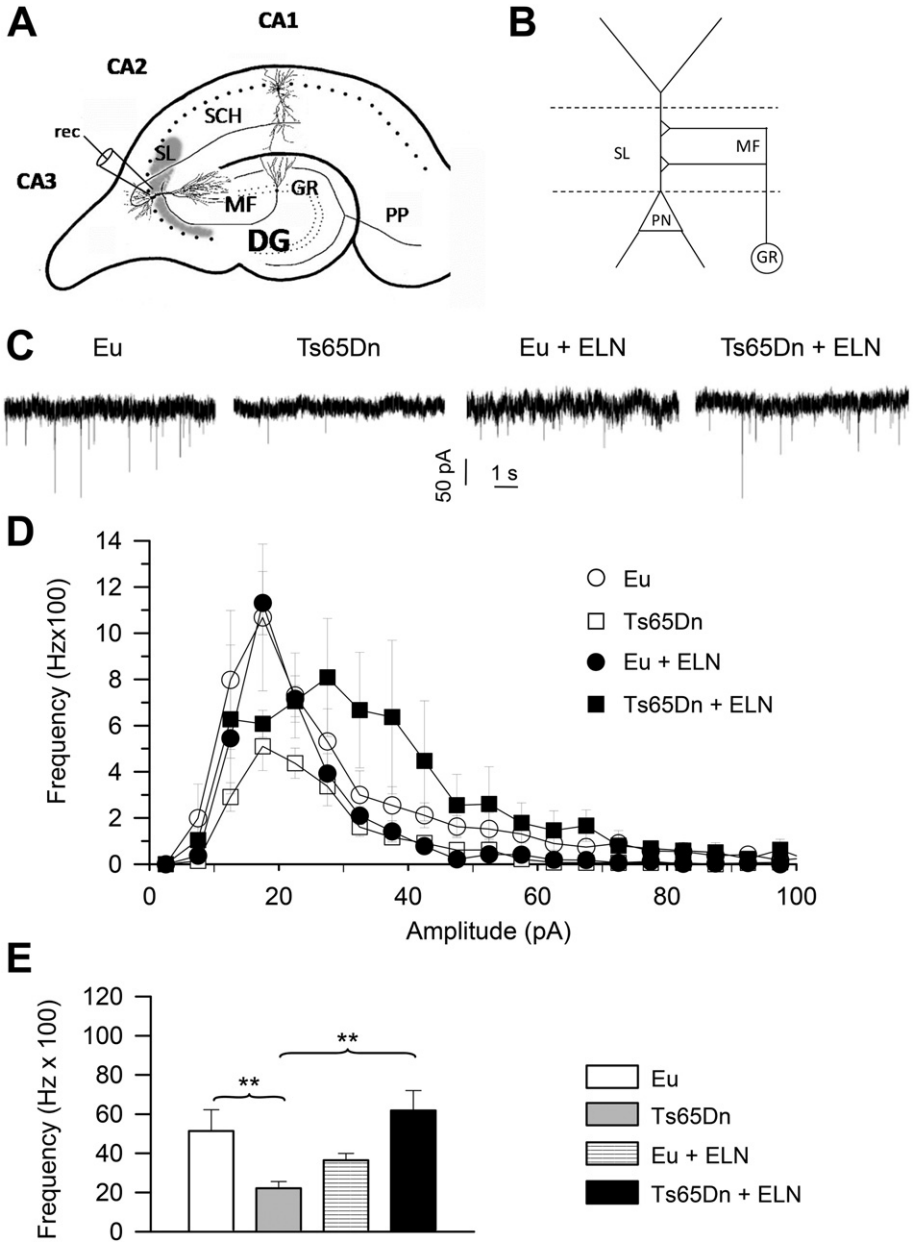

Fig. 7. Long-term effect of treatment with ELN on mEPSC frequency in CA3 pyramidal neurons. A: Schematic drawing of a section across the hippocampal formation showing the major intrinsic connections. Patch clamp recording (rec) of miniature synaptic potentials were carried out from pyramidal neurons of field CA3. The area occupied by the mossy fiber terminals in the stratum lucidum of field CA3 is indicated in gray. B: Mossy fiber circuitry in CA3. Mossy fibers establish excitatory synapses (+) with pyramidal neurons in the stratum lucidum of CA3. C: Exemplary current tracings recorded in the gap-free mode in four representative cells from untreated euploid and Ts65Dn mice and euploid and Ts65Dn mice treated with ELN, showing mEPSC activity. Holding potential was −70 mV. Recordings were made in the presence of 1-μM TTx in the superfusing solution. D: Average frequency-distribution diagrams of mEPSC amplitude for untreated euploid and Ts65Dn mice and euploid and Ts65Dn mice treated with ELN. E: Average, overall mEPSC frequency in the four animal groups. Data derive from 9 untreated euploid mice (13 cells), 7 untreated Ts65Dn mice (18 cells), 8 ELN-treated euploid mice (15 cells), and 4 ELN-treated Ts65Dn mice (12 cells). Values in D-E represent mean ± SE $^{**}p < 0.01$ (Linear mixed model analysis). Abbreviations: CA1–3, hippocampal fields; DG, dentate gyrus; ELN, ELND006; Eu, Euploid; GR, granule cell layer; MF, mossy fibers; PN, pyramidal neuron; PP, perforant pathway; PYR, pyramidal layer; SCH, Shaffer collaterals; SL, stratum lucidum.

averaged among the cells ($n = 2$ to 4), from each animal and then among the animals pertaining to the same experimental group (untreated euploid or Ts65Dn mice, ELN-treated euploid or Ts65Dn mice). The plots thus obtained are shown in Fig. 7D. Consistent with previous evidence (Stagni et al., 2013), in untreated Ts65Dn mice there was a clear reduction in mEPSC frequency for all amplitude classes, with a prominent reduction for amplitudes higher than 35 pA (Fig. 7D). An evaluation of the overall mEPSC frequency showed that in Ts65Dn mice it was reduced by ~53% in comparison with untreated euploid mice (DF = 29; WALD $t = -2.670283$; $p = 0.0123$) (Fig. 7E). In Ts65Dn mice treated with ELN there was a global increase in mEPSC frequency. This increase was particularly prominent for synaptic events of amplitude > 35 pA (Fig. 7E). An evaluation of the overall mEPSC frequency showed that in treated Ts65Dn mice it was increased by ~156% in comparison with untreated Ts65Dn mice (DF = 28; WALD $t = -3.186090$; $p = 0.0035$) and became similar to that of untreated euploid mice (Fig. 7E). In treated euploid mice there was a slight but not statistically significant reduction in the mEPSC frequency in comparison with their untreated counterparts (Fig. 7E).

Results reported in Fig. 7D show that genotype and treatment had differential effects on the frequency of mEPSCs of different magnitude. According to the theory of electrotonic decay of locally generated electric signals, it can be predicted that postsynaptic currents of low magnitude recorded from the soma correspond to the activation of synapses

with a distal dendritic location, while mEPSCs with larger magnitude should mainly correspond to synaptic activation of synapses with a location proximal to the soma. Thus, assuming that mEPSCs kinetics are similar among different synaptic contacts, the mEPSCs of smaller magnitude should display a slower onset and decay kinetics in comparison with mEPSCs of larger amplitude. In order to clarify this issue, we carried out a systematic analysis aimed at correlating mEPSC amplitude and decay kinetics. To this purpose, mEPSCs recorded in each cell and belonging to the same class of amplitude were used to create a single average mEPSC. The decay phase of this average mEPSC was fitted with a single exponential function of the first order, which allowed us to obtain a single value for the decay time constant (τdec). The τdec values obtained for each mEPSCs amplitude class were plotted as a function of the corresponding average amplitude. In all experimental groups, save for the group of untreated Ts65Dn mice, we found a significant inverse relationship between amplitude of the mEPSCs and their τdec (untreated euploid mice: $R = -0.54975$, SD = 1.6319, $n = 24$, $p = 0.00539$; treated euploid mice: $R = -0.40739$, SD = 0.50525, $n = 65$, $p = 7.56715 \times 10^{-4}$; treated Ts65Dn mice: $R = -0.25085$, SD = 0.77471, $n = 148$, $p = 0.0021$), in agreement with the theory of electrotonic decay (Fig. 8).The finding that this was not the case for untreated Ts65Dn mice ($R = 0.03051$, SD = 3.3066, $n = 51$, $p = 0.83168$) suggests that the amplitude heterogeneity of their mEPSCs may be due to additional factors, independent from the distance from the soma. For instance, the shape and size of the dendritic spines may affect the number of postsynaptic receptors and, thus, the magnitude of the mEPSCs.

4. Discussion

4.1. Treatment with ELN has long-term positive effects on neurogenesis in Ts65Dn mice

Ts65Dn mice have a reduced number of granule cell precursors and a reduced number of granule cells starting from prenatal life stages. Repression of the mitogenic Shh pathway by excessive levels of Ptch1 (due to excessive formation of AICD) has been shown to be involved in the reduced proliferation rate of trisomic neural precursor cells (Trazzi et al., 2011). Accordingly, inhibition of the activity of the APP gamma-secretase by ELN reduces AICD formation thereby restoring Ptch1 levels, the number of hippocampal granule cell precursors and total number of granule neurons (Giacomini et al., 2015). In the hippocampal dentate gyrus, granule cells are mainly generated within the first two postnatal weeks, but the number of granule cells increases considerably in the following few weeks (Altman and Bayer, 1975; Altman and Bayer, 1990a, 1990b; Workman et al., 2013). Current results show that at one month after treatment cessation the pool of neural precursor cells was still normalized. Consistently with the long-term restoration of neurogenesis, in treated Ts65Dn mice total number of granule cells was also normalized.

Unlike at P15, at P45 untreated Ts65Dn mice had normal levels of Ptch1. Since Ptch1 transcription in addition of being enhanced by AICD is positively and negatively modulated by other factors (He et al., 2011; Huang et al., 2012; Memmi et al., 2015), the normalization of its

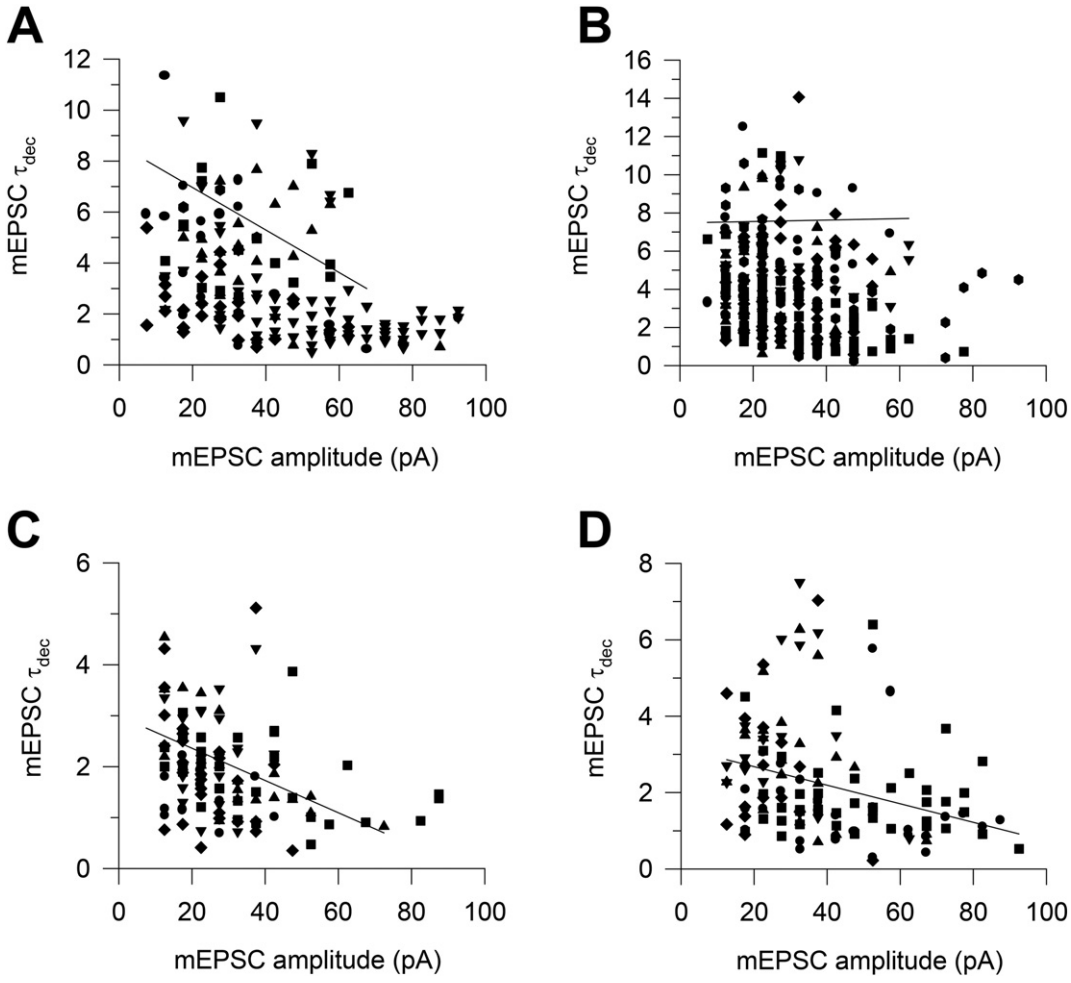

Fig. 8. Correlation between mEPSC amplitude and decay kinetics in untreated and treated euploid and Ts65Dn mice. Scatter plots of mEPSC τdec, obtained by fitting the decay phase of average mEPSCs with a single mono-exponential function, as a function of peak mEPSC amplitude in untreated euploid (A) and Ts65Dn (B) mice and euploid (C) and Ts65Dn (D) mice treated with ELN. Data derive from 9 untreated euploid mice (11 cells), 7 untreated Ts65Dn mice (18 cells), 8 ELN-treated euploid mice (9 cells), and 4 ELN-treated Ts65Dn mice (5 cells).

expression in P45 Ts65Dn mice suggests age-related changes in the mechanisms that regulate its transcription. The finding that untreated P45 Ts65Dn mice still had a reduced pool of neural precursor cells in the DG in spite of normal Ptch1 levels suggests that other perturbed mechanisms, such as enhanced levels of p21 (Fig. 5D) may contribute to neurogenesis impairment. This idea is corroborated by the observation that in treated P45 Ts65Dn mice there was a reduction in p21 levels and a parallel increase of neurogenesis and that in treated euploid mice there was an increase in p21 levels with a reduction of neurogenesis. These findings suggest that inhibition of gamma-secretase in the neonatal period leads to changes in p21 levels that outlast the period of treatment. The mechanisms whereby inhibition of gamma-secretase modulates expression of p21 (and possibly other molecular pathways) remain to be elucidated. The picture emerging from this and previous evidence suggests that the proliferation impairment of trisomic neural precursor cells (NPCs) is due to alteration of various pathways and that alteration of the Shh pathway plays a particularly prominent role during early life stages but that its importance decreases with age.

The finding that in treated euploid mice there was a reduction in the number of NPCs in the DG and in total granule cell number indicates that inhibition of gamma-secretase activity in the normal brain negatively affects the process of neurogenesis. Inhibitors of gamma-secretase are considered strategic tools for Alzheimer's disease because they reduce the formation of Abeta. While the benefit of this approach remains to be clearly demonstrated, from our results it appears that inhibition of gamma-secretase may negatively impact on neurogenesis and connectivity in the non-trisomic brain.

4.2. Treatment with ELN has long-term positive effects on connectivity in field CA3 of Ts65Dn mice

Evaluation of the pre- and postsynaptic terminals in the molecular layer of the DG showed that at one month after treatment cessation Ts65Dn mice had a slightly larger number of SYN and PSD-95 immunoreactive puncta in comparison with their untreated counterparts but this difference was not statistically significant. In contrast, immediately after the end of treatment Ts65Dn mice had a significantly larger number of both SYN and PSD-95 immunoreactive puncta (Giacomini et al., 2015). These results show that the restoration of connectivity observed in the DG of P15 mice at the end of treatment does not outlive treatment cessation and suggests that continuous treatment may be necessary in order to maintain this effect.

Unlike in the molecular layer of the DG, in the stratum lucidum of field CA3 treated Ts65Dn mice had a number of pre- and postsynaptic terminals that was still larger in comparison with their untreated counterparts and similar to that of untreated euploid mice. The stratum lucidum is the site of termination of the mossy fibers, the axons of the granule cells. The persistence of the effects of treatment on the connectivity in this specific hippocampal region can be accounted for by the fact that treatment induces long-term restoration of total granule cell number and, hence, of axons sent by the granule neurons to CA3.

Patch-clamp recordings from the pyramidal neurons of CA3 showed that in untreated Ts65Dn mice there was an overall reduction in the mEPSCs, indicating impairment in the functional connectivity of field CA3. As suggested by analysis of the decay time constant of mEPSCs (Fig. 8), events of large and small magnitude correspond to synapses close and distant from the soma. The prominent reduction in the frequency of mEPSCs of large amplitude in untreated Ts65Dn mice (Fig. 7D) is thus consistent with loss of synapses proximal to the soma. These synapses derive from the mossy fibers, the axons of the granule cells. This conclusion is in agreement with the reduced number of spines forming the thorny excrescences previously demonstrated in Ts65Dn mice (Stagni et al., 2013) and the reduction of PSD-95 immunoreactive puncta, observed here. The finding that in Ts65Dn mice treated with ELN there was a global increase in mEPSC frequency and that this increase was particularly prominent for synaptic events of large amplitude (Fig. 7D) suggests that treatment had a positive impact on the mossy fiber input to the proximal dendrites of CA3 pyramidal neurons. This is fully in agreement with the observation that treatment increased the number of SYN immunoreactive puncta (presynaptic terminals) and PSD-95 immunoreactive puncta (postsynaptic terminals) in the stratum lucidum of field CA3 and indicates that the restored connections are functionally effective. The observation that in treated euploid mice there was a prominent reduction in the frequency of mEPSCs with large magnitude (Fig. 7D) suggests that treatment has an adverse effect on the input from the mossy fibers.

5. Conclusions

Previous findings showed that inhibition of gamma-secretase activity in the neonatal period rescues proliferation impairment in the DG of Ts65Dn mice (Giacomini et al., 2015). Current findings show that the positive effect of neonatal treatment on neural precursor proliferation and total granule cell number is retained with time and that, consistently with normalization of granule cell number, the synaptic input from the DG to CA3 was also functionally restored. The synapses in the DG, however, did not remain in their restored state. Taken together these results show that inhibition of gamma-secretase in the neonatal period leaves a positive trace on the hippocampal region of Ts65Dn mice although, as suggested by evaluation of the levels of CTFs (Fig. 4C, D), the activity of gamma-secretase is no longer inhibited when mice reach 45 days of age. It seems important to observe that although the effects of ELND006 are no longer visible on its target one month after treatment cessation, the effects on plasticity are still significant, indicating a long-lasting effect of treatment. The overall goal of the studies we have being carrying out during the last few years is to identify potential pharmacotherapies for DS. We used here the same treatment schedule used in previous studies (Bianchi et al., 2010; Guidi et al., 2013; Giacomini et al., 2015; Stagni et al., 2016) because we deem it important to compare different drugs in terms of efficacy and duration of their effects. ELND006 has been used for prevention of Alzheimer's disease but the clinical trial was interrupted due to collateral effects (Hopkins, 2011). Yet, although ELND006 by itself may not be a suitable drug for DS, the current finding that many of the effects of treatment were retained with time provides proof of principle demonstration that early inhibition of gamma-secretase may be exploited for the long-term improvement of brain development. Once new and safe inhibitors of gamma-secretase will be created, these might be exploited in order to pharmacologically improve brain alterations in individuals with DS. It must be observed that although AICD derives from the cleavage of both alfa- and beta-CTFs, the amyloidogenic cleavage pathway of APP is predominantly responsible for AICD-mediated nuclear signaling (Goodger et al., 2009). BACE1 inhibitors are considered promising means to reduce Abeta levels in Alzheimer's disease (Yan and Vassar, 2014). Current results suggest that it may be worthwhile to explore the possibility to use inhibitors of BACE1 (Goodger et al., 2009) or antibodies against BACE1 (Dorresteijn et al., 2015) in models of DS, in order to reduce the formation of beta-CTFs and, thus, of AICD, thereby preventing the adverse effects of excessive AICD levels on brain development. Interestingly, recent evidence shows that an anti-Abeta immunotherapeutic approach counteracts Abeta-related pathology in a mouse model of DS (Belichenko et al., 2016). This suggests that a vaccine against AICD may be used in order to inhibit its activity and, thus, its negative effects. This approach would circumvent the difficulties of identifying safe inhibitors of gamma-secretase.

Conflict of interest

The authors declare that they have no conflict of interest.

Acknowledgment

This work was supported by grants to R. B. from Fondazione Telethon (GGP12149), "Fondation Jérôme Lejeune" and "Fondazione del Monte", Italy. The authors are thankful to Dr. Guriqbal S. Basi for his scientific advice. The assistance of Melissa Stott in the revision of the language and the technical assistance of Mr. Francesco Campisi and Mr. Massimo Verdosci is gratefully acknowledged.

References

Altman, J., Bayer, S., 1975. Postnatal development of the hippocampal dentate gyrus under normal and experimental conditions. In: Isaacson, R.L., Pribram, K.H. (Eds.), The Hippocampus. 1. Plenum Press, New York and London, pp. 95–122.

Altman, J., Bayer, S.A., 1990a. Migration and distribution of two populations of hippocampal granule cell precursors during the perinatal and postnatal periods. J. Comp. Neurol. 301, 365–381.

Altman, J., Bayer, S.A., 1990b. Mosaic organization of the hippocampal neuroepithelium and the multiple germinal sources of dentate granule cells. J. Comp. Neurol. 301, 325–342.

Bartesaghi, R., Guidi, S., Ciani, E., 2011. Is it possible to improve neurodevelopmental abnormalities in Down syndrome? Rev. Neurosci. 22, 419–455.

Basi, G.S., Hemphill, S., Brigham, E.F., Liao, A., Aubele, D.L., Baker, J., Barbour, R., Bova, M., Chen, X.H., Dappen, M.S., Eichenbaum, T., Goldbach, E., Hawkinson, J., Lawler-Herbold, R., Hu, K., Hui, T., Jagodzinski, J.J., Keim, P.S., Kholodenko, D., Latimer, L.H., Lee, M., Marugg, J., Mattson, M.N., McCauley, S., Miller, J.L., Motter, R., Mutter, L., Neitzel, M.L., Ni, H., Nguyen, L., Quinn, K., Ruslim, L., Semko, C.M., Shapiro, P., Smith, J., Soriano, F., Szoke, B., Tanaka, K., Tang, P., Tucker, J.A., Ye, X.M., Yu, M., Wu, J., Xu, Y.Z., Garofalo, A.W., Sauer, J.M., Konradi, A.W., Ness, D., Shopp, G., Pleiss, M.A., Freedman, S.B., Schenk, D., 2010. Amyloid precursor protein selective gamma-secretase inhibitors for treatment of Alzheimer's disease. Alzheimers Res. Ther. 2, 36.

Belichenko, P.V., Madani, R., Rey-Bellet, L., Pihlgren, M., Becker, A., Plassard, A., Vuillermot, S., Giriens, V., Nosheny, R.L., Kleschevnikov, A.M., Valletta, J.S., Bengtsson, S.K.S., Linke, G.R., Maloney, M.T., Hickman, D.T., Reis, P., Granet, A., Mlaki, D., Lopez-Deber, M.P., Do, L., Singhal, N., Masliah, E., Pearn, M.L., Pfeifer, A., Muhs, A., Mobley, W.C., 2016. An anti-beta-amyloid vaccine for treating cognitive deficits in a mouse model of down syndrome. PLoS One 11, e0152471.

Bianchi, P., Ciani, E., Guidi, S., Trazzi, S., Felice, D., Grossi, G., Fernandez, M., Giuliani, A., Calza, L., Bartesaghi, R., 2010. Early pharmacotherapy restores neurogenesis and cognitive performance in the Ts65Dn mouse model for Down syndrome. J. Neurosci. 30, 8769–8779.

Brigham, E., Quinn, K., Kwong, G., Willits, C., Goldbach, E., Motter, R., Lee, M., Hu, K., Wallace, W., Kholodenko, D., Tanaka, P., Ni, H., Hemphill, S., Chen, X., Eichenbaum, T., Ruslim, L., Nguyen, L., Santiago, P., Liao, A., Soriano, F., Bova, M., Probst, G., Dappen, M., Latime, R.L., Jagodzinski, J., Konrad, I.A., Garofalo, A., Webb, S., Sham, H., Wehner, N., Tonn, G., Sauer, J., Basi, G., Ness, D., 2010. Pharmacokinetic and pharmacodynamic investigation of ELND006, a novel APP-selective gamma-secretase inhibitor, on amyloid-β concentrations in the brain, CSF and plasma of multiple nonclinical species following oral administration. International Conference on Alzheimer's Disease, Honolulu, 2010.

Castelli, L., Nigro, M.J., Magistretti, J., 2007. Analysis of resurgent sodium-current expression in rat parahippocampal cortices and hippocampal formation. Brain Res. 1163, 44–55.

Costa, A.C., Scott-McKean, J.J., 2013. Prospects for improving brain function in individuals with down syndrome. CNS Drugs 27, 679–702.

Cupers, P., Orlans, I., Craessaerts, K., Annaert, W., De Strooper, B., 2001. The amyloid precursor protein (APP)-cytoplasmic fragment generated by gamma-secretase is rapidly degraded but distributes partially in a nuclear fraction of neurones in culture. J. Neurochem. 78, 1168–1178.

Dierssen, M., 2012. Down syndrome: the brain in trisomic mode. Nat. Rev. Neurosci. 13, 844–858.

Dorresteijn, B., Rotman, M., Faber, D., Schravesande, R., Suidgeest, E., van der Weerd, L., van der Maarel, S.M., Verrips, C.T., El Khattabi, M., 2015. Camelid heavy chain only antibody fragment domain against beta-site of amyloid precursor protein cleaving enzyme 1 inhibits beta-secretase activity in vitro and in vivo. FEBS J. 282, 3618–3631.

Engidawork, E., Gulesserian, T., Seidl, R., Cairns, N., Lubec, G., 2001. Expression of apoptosis related proteins: RAIDD, ZIP kinase, Bim/BOD, p21, Bax, Bcl-2 and NF-kappaB in brains of patients with Down syndrome. J. Neural Transm. Suppl. 181–192.

Gardiner, K.J., 2015. Pharmacological approaches to improving cognitive function in Down syndrome: current status and considerations. Drug Des. Devel. Ther. 9, 103–125.

Giacomini, A., Stagni, F., Trazzi, S., Guidi, S., Emili, M., Brigham, E., Ciani, E., Bartesaghi, R., 2015. Inhibition of APP gamma-secretase restores Sonic Hedgehog signaling and neurogenesis in the Ts65Dn mouse model of Down syndrome. Neurobiol. Dis. 82, 385–396.

Goodger, Z.V., Rajendran, L., Trutzel, A., Kohli, B.M., Nitsch, R.M., Konietzko, U., 2009. Nuclear signaling by the APP intracellular domain occurs predominantly through the amyloidogenic processing pathway. J. Cell Sci. 122, 3703–3714.

Guidi, S., Stagni, F., Bianchi, P., Ciani, E., Ragazzi, E., Trazzi, S., Grossi, G., Mangano, C., Calza, L., Bartesaghi, R., 2013. Early pharmacotherapy with fluoxetine rescues dendritic pathology in the Ts65Dn mouse model of Down syndrome. Brain Pathol. 23, 129–143.

Guidi, S., Stagni, F., Bianchi, P., Ciani, E., Giacomini, A., De Franceschi, M., Moldrich, R., Kurniawan, N., Mardon, K., Giuliani, A., Calza, L., Bartesaghi, R., 2014. Prenatal pharmacotherapy rescues brain development in a Down's syndrome mouse model. Brain 137, 380–401.

Hamill, O.P., Marty, A., Neher, E., Sakmann, B., Sigworth, F.J., 1981. Improved patch-clamp techniques for high-resolution current recording from cells and cell-free membrane patches. Pflugers Arch. 391, 85–100.

He, Z., Cai, J., Lim, J.-W., Kroll, K., Ma, L., 2011. A novel KRAB domain-containing zinc finger transcription factor ZNF431 directly represses Patched1 transcription. J. Biol. Chem. 286, 7279–7289.

Hopkins, C.R., 2011. ACS chemical neuroscience molecule spotlight on ELND006: another gamma-secretase inhibitor fails in the clinic. ACS Chem. Neurosci. 2, 279–280.

Huang, G.J., He, Z., Ma, L., 2012. ZFP932 suppresses cellular Hedgehog response and Patched1 transcription. Vitam. Horm. 88, 309–332.

Kempermann, G., Gage, F.H., 2002. Genetic influence on phenotypic differentiation in adult hippocampal neurogenesis. Brain Res. Dev. Brain Res. 134, 1–12.

Malberg, J.E., Eisch, A.J., Nestler, E.J., Duman, R.S., 2000. Chronic antidepressant treatment increases neurogenesis in adult rat hippocampus. J. Neurosci. 20, 9104–9110.

Memmi, E.M., Sanarico, A.G., Giacobbe, A., Peschiaroli, A., Frezza, V., Cicalese, A., Pisati, F., Tosoni, D., Zhou, H., Tonon, G., Antonov, A., Melino, G., Pelicci, P.G., Bernassola, F., 2015. p63 sustains self-renewal of mammary cancer stem cells through regulation of Sonic Hedgehog signaling. Proc. Natl. Acad. Sci. U. S. A. 112, 3499–3504.

Park, J., Oh, Y., Yoo, L., Jung, M.S., Song, W.J., Lee, S.H., Seo, H., Chung, K.C., 2010. Dyrk1A phosphorylates p53 and inhibits proliferation of embryonic neuronal cells. J. Biol. Chem. 285, 31895–31906.

Probst, G., Aubele, D.L., Bowers, S., Dressen, D., Garofalo, A.W., Hom, R.K., Konradi, A.W., Marugg, J.L., Mattson, M.N., Neitzel, M.L., Semko, C.M., Sham, H.L., Smith, J., Sun, M., Truong, A.P., Ye, X.M., Xu, Y.Z., Dappen, M.S., Jagodzinski, J.J., Keim, P.S., Peterson, B., Latimer, L.H., Quincy, D., Wu, J., Goldbach, E., Ness, D.K., Quinn, K.P., Sauer, J.M., Wong, K., Zhang, H., Zmolek, W., Brigham, E.F., Kholodenko, D., Hu, K., Kwong, G.T., Lee, M., Liao, A., Motter, R.N., Sacayon, P., Santiago, P., Willits, C., Bard, F., Bova, M.P., Hemphill, S.S., Nguyen, L., Ruslim, L., Tanaka, K., Tanaka, P., Wallace, W., Yednock, T.A., Basi, G.S., 2013. Discovery of (R)-4-cyclopropyl-7,8-difluoro-5-(4-(trifluoromethyl)phenylsulfonyl)-4,5-dihydro- 1H-pyrazolo[4,3-c]quinoline (ELND006) and (R)-4-cyclopropyl-8-fluoro-5-(6-(trifluoromethyl)pyridin-3-ylsulfonyl)-4,5-dihydr o-2H-pyrazolo[4,3-c]quinoline (ELND007): metabolically stable gamma-secretase inhibitors that selectively inhibit the production of amyloid-beta over notch. J. Med. Chem. 56, 5261–5274.

Reeves, R.H., 2006. Down syndrome mouse models are looking up. Trends Mol. Med. 12, 237–240.

Reeves, R.H., Irving, N.G., Moran, T.H., Wohn, A., Kitt, C., Sisodia, S.S., Schmidt, C., Bronson, R.T., Davisson, M.T., 1995. A mouse model for Down syndrome exhibits learning and behaviour deficits. Nat. Genet. 11, 177–184.

Reinholdt, L.G., Ding, Y., Gilbert, G.J., Czechanski, A., Solzak, J.P., Roper, R.J., Johnson, M.T., Donahue, L.R., Lutz, C., Davisson, M.T., 2011. Molecular characterization of the translocation breakpoints in the Down syndrome mouse model Ts65Dn. Mamm. Genome 22, 685–691.

Roper, R.J., Baxter, L.L., Saran, N.G., Klinedinst, D.K., Beachy, P.A., Reeves, R.H., 2006. Defective cerebellar response to mitogenic Hedgehog signaling in Down [corrected] syndrome mice. Proc. Natl. Acad. Sci. U. S. A. 103, 1452–1456.

Stagni, F., Magistretti, J., Guidi, S., Ciani, E., Mangano, C., Calza, L., Bartesaghi, R., 2013. Pharmacotherapy with fluoxetine restores functional connectivity from the dentate gyrus to field CA3 in the Ts65Dn mouse model of Down syndrome. PLoS One 8, e61689.

Stagni, F., Giacomini, A., Guidi, S., Ciani, E., Bartesaghi, R., 2015. Timing of therapies for Down syndrome: the sooner, the better. Front. Behav. Neurosci. 9, 265.

Stagni, F., Giacomini, A., Emili, M., Trazzi, S., Guidi, S., Sassi, M., Ciani, E., Rimondini, R., Bartesaghi, R., 2016. Short- and long-term effects of neonatal pharmacotherapy with epigallocatechin-3-gallate on hippocampal development in the Ts65Dn mouse model of Down syndrome. Neuroscience 333, 277–301.

Tozuka, Y., Fukuda, S., Namba, T., Seki, T., Hisatsune, T., 2005. GABAergic excitation promotes neuronal differentiation in adult hippocampal progenitor cells. Neuron 47, 803–815.

Trazzi, S., Mitrugno, V.M., Valli, E., Fuchs, C., Rizzi, S., Guidi, S., Perini, G., Bartesaghi, R., Ciani, E., 2011. APP-dependent up-regulation of Ptch1 underlies proliferation impairment of neural precursors in Down syndrome. Hum. Mol. Genet. 20, 1560–1573.

Trazzi, S., Fuchs, C., Valli, E., Perini, G., Bartesaghi, R., Ciani, E., 2013. The amyloid precursor protein (APP) triplicated gene impairs neuronal precursor differentiation and neurite development through two different domains in the Ts65Dn mouse model for Down syndrome. J. Biol. Chem. 288, 20817–20829.

West, M.J., Gundersen, H.J., 1990. Unbiased stereological estimation of the number of neurons in the human hippocampus. J. Comp. Neurol. 296, 1–22.

Workman, A.D., Charvet, C.J., Clancy, B., Darlington, R.B., Finlay, B.L., 2013. Modeling transformations of neurodevelopmental sequences across mammalian species. J. Neurosci. 33, 7368–7383.

Yan, R., Vassar, R., 2014. Targeting the beta secretase BACE1 for Alzheimer's disease therapy. Lancet Neurol. 13, 319–329.

Zheng, C., Gu, X., Zhong, Z., Zhu, R., Gao, T., Wang, F., 2012. Two memory associated genes regulated by amyloid precursor protein intracellular domain: novel insights into the pathogenesis of learning and memory impairment in Alzheimer's disease. Neural Regen. Res. 7, 341–346.